# Equilateral Triangular Array Formation Configuration Initialization Control for Space-Based Gravitational Wave Observatory

PAN Zhengxu<sup>1</sup>, BANDO Mai<sup>2</sup>, ZHU Zhanxia<sup>1\*</sup>, HOKAMOTO Shinji<sup>2</sup>

- 1. School of Astronautics, Northwestern Polytechnical University, Xi'an 710072, P. R. China;
- 2. Department of Aeronautics and Astronautics, Kyushu University, Fukuoka 819-0395, Japan

(Received 8 June 2025; revised 23 July 2025; accepted 29 August 2025)

**Abstract:** This paper presents an analysis of an equilateral triangular array formation initialization for space-based gravitational wave observatory (GWO) near Lagrange points in the circular-restricted three-body problem. A stable configuration is essential for the continuous observation of gravitational waves (GWs). However, the motion near the collinear libration points is highly unstable. This problem is examined by output regulation theory. Using the tracking aspect, the equilateral triangular array formation is established in two periods and the fuel consumption is calculated. Furthermore, the natural evolution of the formation without control input is analyzed, and the effective stability duration is quantified to determine the timing of control interventions. Finally, to observe the GWs in same direction with different frequency bands, scale reconfiguration is employed.

**Key words:** space-based gravitational wave observatory; equilateral triangular array formation initialization; Lagrange point; output regulation theory

**CLC number:** V475.4 **Document code:** A **Article ID:** 1005-1120(2025)S-0012-14

### 0 Introduction

There are many gravitational wave sources in the universe. Gravitational waves (GWs) are theoretically predicted by Einstein's field equations<sup>[1]</sup>. The gravitational wave observatory (GWO) missions are of great significance for verifying the theory of relativity and exploring the origin of the universe<sup>[2]</sup>. Laser interferometer gravitational-wave observatory (LIGO) successfully observed GW signals for the first time in 2015, thereby ushering in a new era in the study of the universe based on GWs<sup>[3]</sup>. GWOs can be categorized ground-based GWOs and space-based GWOs. Ground-based GWOs include LIGO<sup>[3]</sup>, TA-MA300<sup>[4]</sup>, and GEO600<sup>[5]</sup>. Ground-based GWOs only observe high-frequency GWs due to the limitation of arm length and noise interference. As a re-

they cannot access the medium- and low-frequency bands, where a wealth of astrophysical sources such as massive black hole binaries, extreme mass-ratio inspirals, and stochastic backgrounds are expected to exist. To overcome these limitations, space-based GWOs employing spacecraft formation flying are preferred. The European Space Agency (ESA) and the National Aeronautics and Space Administration (NASA) first proposed the laser interferometer space antenna (LISA) in 1993<sup>[6]</sup>. Since then, numerous GWO mission concepts have been proposed, including DECIGO<sup>[7]</sup>, BBO<sup>[8]</sup>, TianQin<sup>[9]</sup>, and Taiji<sup>[10]</sup>. The basic principle of a space-based GWO is to employ three spacecraft arranged in an equilateral triangular formation. To date, three effective mechanisms for realizing such triangular formations have been proposed: Co-orbital constellation, relative orbit, and triangu-

**How to cite this article**: PAN Zhengxu, BANDO Mai, ZHU Zhanxia, et al. Equilateral triangular array formation configuration initialization control for space-based gravitational wave observatory [J]. Transactions of Nanjing University of Aeronautics and Astronautics, 2025, 42(S): 12-25.

<sup>\*</sup>Corresponding author, E-mail address: zhuzhanxia@nwpu.edu.cn.

lar libration point<sup>[2]</sup>.

The process of establishing an equilateral triangular formation is referred to as formation initialization. Although an equilateral triangular configuration is essential for GWOs, relatively few studies have focused on this problem. Several studies have proposed equilateral triangular formation design methods based on orbital geometric relationships<sup>[11-12]</sup>. In Ref. [13], a space circular formation was constructed using the Clohessy-Wiltshire (CW) equation. Since the CW equation has only first-order accuracy, Jiao et al. [14] proposed a spatial circular configuration design based on the second-order CW equation. Additionally, Liu et al. [15] proposed a geometric formation design method also based on the CW equation. To ensure long-term stability of the configuration, various optimization methods have also been investigated. Xia et al.[16] optimized the natural orbital configuration of LISA using a hybrid reactive tabu search algorithm. In Ref.[17], an adaptive solution space adjustment algorithm was proposed to enhance the convergence efficiency of the differential evolution (DE) algorithm. Regarding configuration initialization, some studies have investigated the use of impulse maneuvers to guide each spacecraft into its designated position<sup>[16,18]</sup>.

Currently, various control methods can be employed for spacecraft initialization, among which output regulation theory is often preferred due to its straightforward design and computational efficiency<sup>[19]</sup>. Output regulation theory is a control theory that aims to regulate the output of a system to follow a desired reference signal, even in the presence of disturbances and uncertainties. In the field of spacecraft formation, this theory has been applied to various formation problems, ranging from near-Earth formations to Lagrange point formations<sup>[20-22]</sup>.

This paper presents an analysis of the equilateral triangular array formation near the Sun-Earth Lagrange points, and a control strategy for a precise equilateral triangular array formation that can be applied to the Sun-Earth Lagrange points is proposed. The fuel consumption for maintaining the formation

at the collinear libration points is evaluated. Furthermore, the uncontrolled evolution of the equilateral triangular array formation is examined, and the effective stability duration is quantified to determine how long the equilateral triangular array formation configuration can remain intact without intervention. To observe GWs in the same direction with different frequency bands, reconfiguration control is performed.

### 1 Equations of Motion in CRTBP

In this study, the circular restricted three-body problem (CRTBP) is employed to describe the motion of a spacecraft P, under the gravitational influence of two massive celestial bodies,  $M_1$  and  $M_2$ , which represent the Sun and the Earth, respectively, as illustrated in Fig.1. The non-dimensional coordinates of the spacecraft, Sun, and Earth are given by (X,Y,Z),  $(-\rho,0,0)$ , and  $(1-\rho,0,0)$ , respectively. The equations of motion of the spacecraft in non-dimensional form are provided in Ref. [22].

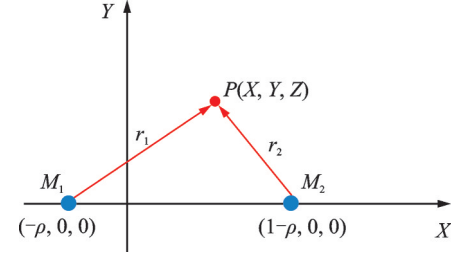


Fig.1 CRTBP system

$$\begin{cases} \ddot{X} - 2\dot{Y} - X = -\frac{1-\rho}{r_1^3} (X+\rho) - \\ \frac{\rho}{r_2^3} (X-1+\rho) + u_x \\ \ddot{Y} + 2\dot{X} - Y = -\frac{1-\rho}{r_1^3} Y - \frac{\rho}{r_2^3} Y + u_y \\ \ddot{Z} = -\frac{1-\rho}{r_1^3} Z - \frac{\rho}{r_2^3} Z + u_z \end{cases}$$
(1)

where the mass parameter  $\rho = \frac{M_2}{M_1 + M_2}$  and  $(u_x, u_y, u_z)$  represent the control accelerations in the X, Y, and Z directions, respectively. The distances between the spacecraft and the two primary bodies

are denoted by  $r_1$  and  $r_2$ , as follows

$$r_1 = \sqrt{(X+\rho)^2 + Y^2 + Z^2}$$
 $r_2 = \sqrt{(X-1+\rho)^2 + Y^2 + Z^2}$ 

The equations of motion are normalized, therefore, Eq.(1) includes stationary points known as Lagrange points,  $L_i$ , which satisfy

$$\begin{cases} X = \frac{1 - \rho}{r_1^3} (X + \rho) + \frac{\rho}{r_2^3} (X - 1 + \rho) \\ Y = \frac{1 - \rho}{r_1^3} Y + \frac{\rho}{r_2^3} Y \\ Z = 0 \end{cases}$$
 (2)

and the positions of the Lagrange points are given by

$$\begin{cases}
L_{1} = (l_{1}(\rho), 0, 0) \\
L_{2} = (l_{2}(\rho), 0, 0) \\
L_{3} = (l_{3}(\rho), 0, 0) \\
L_{4} = (1/2 - \rho, \sqrt{3}/2, 0) \\
L_{5} = (1/2 - \rho, -\sqrt{3}/2, 0)
\end{cases}$$
(3)

where the values of  $l_i$  are determined by Eq.(3). To describe the equations of motion near a collinear libration point  $L_i$  (i=1,2,3), it is convenient to use the coordinate system with its center located at  $L_i$ . Replacing X, Y, and Z by  $x+l_i$ , y, z, Eq.(1) can be rewritten as

$$\begin{cases} \ddot{x} - 2\dot{y} - x = l_i - \frac{1 - \rho}{r_1^3} (x + l_i + \rho) - \\ \frac{\rho}{r_2^3} (x + l_i - 1 + \rho) + u_x \\ \ddot{y} + 2\dot{x} - y = -\frac{1 - \rho}{r_1^3} y - \frac{\rho}{r_2^3} y + u_y \\ \ddot{z} = -\frac{1 - \rho}{r_1^3} z - \frac{\rho}{r_2^3} z + u_z \end{cases}$$
(4)

where

$$r_1 = \sqrt{(x + l_i + \rho)^2 + y^2 + z^2}$$
 $r_2 = \sqrt{(x + l_i - 1 + \rho)^2 + y^2 + z^2}$ 

Linearized equations in Eq.(4) at the origin are expressed as

$$\begin{cases}
\ddot{x} - 2\dot{y} - (2\sigma_i + 1) x = u_x \\
\ddot{y} + 2\dot{x} + (\sigma_i - 1) y = u_y
\end{cases}$$

$$\ddot{z} + \sigma_i z = u_z$$
(5)

where

$$\sigma_{i} = \frac{\rho}{\left|l_{i}(\rho) - 1 + \rho\right|^{3}} + \frac{1 - \rho}{\left|l_{i}(\rho) + \rho\right|^{3}}$$

Then, Eq.(5) can be rewritten in the state space form as

$$\dot{x} = Ax + Bu \tag{6}$$

where

$$A = \begin{bmatrix} x & y & \dot{x} & \dot{y} & z & \dot{z} \end{bmatrix}^{\mathsf{T}} \quad \mathbf{u} = \begin{bmatrix} u_x & u_y & u_z \end{bmatrix}^{\mathsf{T}}$$

$$A = \begin{bmatrix} 0 & 0 & 1 & 0 & 0 & 0 \\ 0 & 0 & 0 & 1 & 0 & 0 \\ 2\sigma_i + 1 & 0 & 0 & 2 & 0 & 0 \\ 0 & 1 - \sigma_i & -2 & 0 & 0 & 0 \\ 0 & 0 & 0 & 0 & 0 & 1 \\ 0 & 0 & 0 & 0 & -\sigma_i & 0 \end{bmatrix}$$

$$\begin{bmatrix} 0 & 0 & 0 \end{bmatrix}$$

$$B = \begin{bmatrix} 0 & 0 & 0 \\ 0 & 0 & 0 \\ 1 & 0 & 0 \\ 0 & 1 & 0 \\ 0 & 0 & 0 \\ 0 & 0 & 1 \end{bmatrix}$$

Similarly, the state-space form of Eq.(6) can be written in a semi-linear form as

$$\dot{x} = Ax + Bf(x) + Bu$$

where f(x) represents the nonlinear component, expressed as

$$f(x) = \begin{bmatrix} l_i - 2\sigma_i x - \frac{1-\rho}{r_1^3} (x + l_i + \rho) - \frac{\rho}{r_2^3} (x + l_i - 1 + \rho) \\ \sigma_i y - \frac{1-\rho}{r_1^3} y - \frac{\rho}{r_2^3} y \\ \sigma_i z - \frac{1-\rho}{r_1^3} z - \frac{\rho}{r_2^3} z \end{bmatrix} = \begin{bmatrix} f_x \\ f_y \\ f_z \end{bmatrix}$$

### 2 Output Regulation Problem

In the initialization and configuration design of spacecraft formations for space-based GWOs, main-

taining a prescribed geometric configuration with high precision is of paramount importance, and this requirement can be naturally formulated as an output regulation problem. Output regulation theory provides a systematic and effective framework to address this challenge, as it not only guarantees closed-loop stability but also ensures asymptotic tracking of reference trajectories and rejection of external disturbances, even in the presence of nonlinear dynamics and perturbations<sup>[19]</sup>. In this section, a general output regulation problem is reviewed with the focus placed on state-feedback formulations. Within this framework, the designed controller enables spacecraft to be steered accurately from their initial states to the desired equilateral triangular formation, and to preserve this configuration over the long term by compensating for persistent perturbations. This capability is critical for supporting the stringent interferometric measurement requirements of GWOs.

Let us consider a general system defined as follows

$$\begin{cases}
\dot{\tilde{x}} = A\tilde{x} + B_1 w + B_2 u \\
\tilde{z} = C_1 \tilde{x} + D_{11} w + D_{12} u \\
\tilde{y} = C_2 \tilde{x} + D_{21} w
\end{cases} (7)$$

where  $\tilde{x} \in \mathbb{R}^n$  is the state, initial value  $\tilde{x}(0)$  is given and all the matrices are T-periodic;  $u \in \mathbb{R}^m$  is control input,  $\tilde{z} \in \mathbb{R}^q$  the output to be regulated, and  $\tilde{y} \in \mathbb{R}^p$  an observation available to the controller; the exogenous signal  $w \in \mathbb{R}^s$  is generated by a periodic anti-stable exogenous system as follows

$$\begin{cases}
\dot{\boldsymbol{w}} = S\boldsymbol{w} \\
\boldsymbol{w}(0) = \boldsymbol{w}_0
\end{cases} \tag{8}$$

The primary challenge in an output regulation problem is to design a stable periodic output feedback controller that drives  $\tilde{z}(t)$  to zero, regardless of the initial conditions  $\tilde{x}(0)$  and w(0). To address this, several standard assumptions and theorems are necessary.

Assumption 1  $(A, B_2)$  is stabilizable, for a periodic system, its monodromy matrix is stable, that is, all of its eigenvalues (Floquet multipliers) lie within the unit circle of the complex plane.

Assumption 2 
$$\begin{bmatrix} (C_2 & D_{21}) & \begin{pmatrix} A & B_1 \\ 0 & S \end{bmatrix} \end{bmatrix}$$
 is de-

tectable.

Assumption 3 The exosystem is naturally stable, that is, all eigenvalues of the matrix S are simple eigenvalues located on the imaginary axis,

with algebraic multiplicities equal to geometric multiplicities.

**Remark** It should be emphasized that Assumptions 1-3 can be satisfied in the proposed framework. Specifically, Assumption 1 requires the monodromy matrix of the periodic system to be stable. This condition is ensured by selecting appropriate periodic orbits under the CRTBP model and designing a periodic feedback gain based on the output regulation theory, such that the closed-loop Floquet multipliers lie inside the unit circle. In Assumption 2, the solvability of the regulator equations requires the extended system to satisfy the observability condition, together with the compatibility condition of the exosystem. From a physical perspective, this means that all unstable modes of the plant and the exosystem can be reconstructed from the chosen outputs. Here, the outputs are defined as the relative position errors of the spacecraft, ensuring the observability of the extended system. Finally, Assumption 3 requires the exosystem to be neutrally stable. In this study, the exosystem is constructed to generate the periodic reference signals of the equilateral triangular formation, whose eigenvalues are purely imaginary and simple, thereby naturally fulfilling the neutral stability condition. Therefore, Assumptions 1-3 are all satisfied in the spacecraft formation control problem considered in this work, providing the theoretical foundation for applying output regulation theory.

Assuming that Assumptions 1-3 hold, the solvability of the control problem and the design of a controller capable of achieving output tracking can be characterized by the output regulation equations, that is the output regulation problem defined by Eq.(7) is solvable, if and only if there exist matrices  $\mathbf{\Pi}$  and  $\mathbf{\Gamma}$  which solve Eq.(9) often called the regulator equation.

$$\begin{cases}
A\mathbf{\Pi} - \mathbf{\Pi}S + B_1 + B_2\mathbf{\Gamma} = 0 \\
C_1\mathbf{\Pi} + D_{11} + D_{12}\mathbf{\Gamma} = 0
\end{cases}$$
(9)

#### **Proof**

Consider the periodic system (Eq.(7)), in which all matrices are T-periodic. An augmented system is introduced to incorporate periodicity directly into the state-space formulation, thereby facil-

itating further analysis of the system's periodic properties. The augmented state vector is defined as

$$\boldsymbol{\xi} = [\tilde{\boldsymbol{x}}^{\mathrm{T}}, \boldsymbol{w}^{\mathrm{T}}]^{\mathrm{T}}$$

Accordingly, the dynamics of the system can be rewritten as

$$\ddot{\boldsymbol{\xi}} = \begin{bmatrix} A & B_1 \\ 0 & S \end{bmatrix} \boldsymbol{\xi} + \begin{bmatrix} B_2 \\ 0 \end{bmatrix} \boldsymbol{u}$$
 $\tilde{\boldsymbol{z}} = \begin{bmatrix} C_1 & D_{11} \end{bmatrix} \boldsymbol{\xi} + D_{12} \boldsymbol{u}$ 

The periodic system is reformulated as an augmented linear system, whose characteristics are determined by the T-periodic matrices and derived from the dynamics of the exosystem. The objective of output regulation is to design the control input usuch that  $\tilde{z}(t) \rightarrow 0$  as  $t \rightarrow \infty$ , regardless of the initial disturbance. This requirement leads to the necessity of solving the output regulation equation (Eq.(9)). Here, the matrix  $\mathbf{\Pi}$  maps the disturbance state  $\mathbf{w}$  to the system state  $\tilde{x}$ , while the matrix  $\Gamma$  determines the control law to achieve disturbance rejection or reference tracking. If the augmented system satisfies Assumptions 1—3, the system is controllable and observable, and the output regulation equations admit a solution. Therefore, Assumptions 1-3 ensure the existence of a solution ( $\Pi, \Gamma$ ) to the regulator equations. Subsequently, the monodromy matrix of the periodic system is analyzed using Floquet theory. When the control input is given in the form of a periodic feedback law, it can be expressed as

$$u(t) = K(t) \tilde{y}(t)$$

where K(t) is a periodic matrix. In the closed-loop system, the dynamics of the augmented state can be expressed as

$$\dot{\boldsymbol{\xi}} = \begin{bmatrix} A + B_2 K(t) & B_1 \\ 0 & S \end{bmatrix} \boldsymbol{\xi}$$

According to Floquet theory, the stability of a periodic system is determined by the state transition matrix over one period, namely the monodromy matrix. If all Floquet multipliers (i.e., the eigenvalues of the monodromy matrix) lie within the unit circle of the complex plane, the system is stable. By properly designing K(t), the stability of the closed-loop system can be ensured.

According to Assumption 3, the matrix  $\boldsymbol{S}$  is neutrally stable, with its eigenvalues located on the imaginary axis and with algebraic multiplicities

equal to their geometric multiplicities. Under this condition, the solution pair  $(\boldsymbol{H}, \boldsymbol{\Gamma})$  can be employed to design the control law, thereby ensuring that  $\tilde{\boldsymbol{z}}(t) \rightarrow 0$  and enabling the system to achieve both disturbance rejection and reference tracking.

### 3 Equilateral Triangular Array Formation Based on Output Regulation Theory

In this section, the design of the GWO array formation configuration is presented. Traditionally, a GWO formation consists of three spacecraft, and its arm length determines the frequency range of the GWO. Due to the extremely weak intensity of GWs, the noise level of the laser interferometer is subject to a notably high noise level; therefore, sensitivity is regarded as a critical performance parameter. Additional assumptions are introduced in this section.

Assumption 4 The variation in arm length induced by GWs is proportional to both the nominal arm length as well as to the amplitude and frequency of GWs.

Assumption 5 The detector's sensitivity is directly determined by the variation in arm length, which is proportional to the nominal arm length. There exists an optimal nominal arm length that maximizes the detector's sensitivity within a specific target frequency band.

Assumption 6 The perturbation of the spacetime metric tensor caused by GWs is assumed to be linear; that is, smaller (or larger) GW perturbations lead to proportionally smaller(or larger) variations in arm length. These variations depend on both the strength and frequency of GWs.

Based on the above assumptions, let the arm length of the interferometer be denoted by L. When GWs arrive, their effect causes one arm to elongate while the other arm contracts perpendicularly. Let  $\Delta L$  represent the variation in arm length. Consequently, the two arms become  $L + \Delta L$  and  $L - \Delta L$ , respectively. The sensitivity, denoted by  $h_d$ , is defined as

$$h_{\rm d} = \frac{\Delta L}{L} \tag{10}$$

In Eq.(10), since  $\Delta L$  is much smaller than L, the sensitivity decreases as the arm length increases. To enhance sensitivity and mitigate laser attenuation, array formations are introduced. In this paper, the equilateral triangular array formation is introduced, as illustrated in Fig.2.

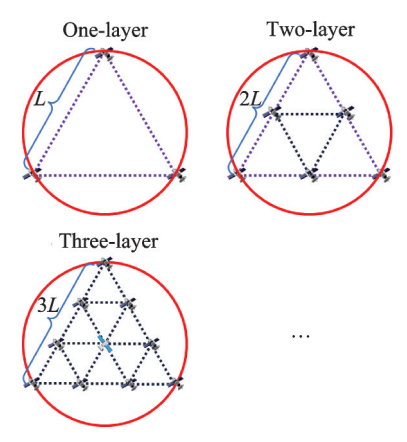


Fig.2 Equilateral triangular array formation

In Fig.2, one-layer, two-layer and three-layer equilateral triangular array formations are designed. Multiple spacecraft are deployed on each side, forming a "nested" configuration. This method effectively mitigates laser attenuation and enables longer baselines.

Then, the control law is derived to establish and maintain the equilateral triangular array formation using the output regulation theory. If the orbit of the follower spacecraft, which exhibits a periodic orbit described by a sinusoidal function, is chosen as a reference, the equilateral triangular array formation can be achieved in a given period. Consider a triangular array formation in which the leader spacecraft is located near the  $L_i$  point, as described by Eq.(11) and the reference orbit of the follower spacecraft is  $x_l+w=(x_l+w_1,y_l+w_2,z_l+w_3)$ . Here  $(w_1,w_2,w_3)$  denotes a periodic relative orbit of the follower spacecraft

$$\dot{\boldsymbol{x}}_{l} = A\boldsymbol{x}_{l} + B\boldsymbol{f}(\boldsymbol{x}_{l}) \quad \boldsymbol{x}_{l}(0) = \boldsymbol{x}_{l0} \tag{11}$$

where  $x_i$  represents a periodic orbit of the leader spacecraft near the Lagrange point  $L_i$ . For

$$(w_1, w_2, w_3)$$
, it is given by

$$\begin{cases} w_{1}(t) = a\cos(\omega_{1}t + \tau_{i}) \\ w_{2}(t) = 2a\sin(\omega_{1}t + \tau_{i}) \\ w_{3}(t) = \sqrt{3} a\cos(\omega_{2}t + \tau_{i}) \\ \tau_{i} = 0, \frac{2}{3}\pi, \frac{4}{3}\pi; i = 1, 2, 3 \end{cases}$$
(12)

The trajectory (defined by Eq.(12)) is generated as follows

$$\dot{\boldsymbol{w}} = \boldsymbol{S} \boldsymbol{w} \quad \boldsymbol{w}(0) = \boldsymbol{w}_0 \tag{13}$$

where

$$S = \begin{bmatrix} 0 & s_1 & 0 & 0 \\ s_2 & 0 & 0 & 0 \\ 0 & 0 & 0 & 1 \\ 0 & 0 & -\omega_2^2 & 0 \end{bmatrix}$$

$$s = -\frac{\omega_1}{2} \quad s_2 = 2\omega_2 \quad \omega > 0$$

Given the general system described by Eq.(7) and exogenous system described by Eq.(8), the output regulation problem aims to find a control law such that  $\tilde{z}(t)$  converges to zero as time approaches infinity for any initial conditions of the exosystem. According to Assumption 1 and Eq.(9), admissible controllers are given by

$$\boldsymbol{u} = -F\boldsymbol{x} + (\boldsymbol{\Gamma} + F\boldsymbol{\Pi})\boldsymbol{w} \tag{14}$$

where F is an arbitrary feedback gain such that A-BF is asymptotically stable. Likewise, the triangular array formation problem for the semi-linear system can be solved by the nonlinear feedback control given by

 $u = -Fe + f(x_t) - f(x) + (\mathbf{\Gamma} + F\mathbf{\Pi}) w$  (15) where  $e = x - x_t$ . If the full state is available (x = y), Eq.(9) is rewritten as follows

$$\begin{cases}
A\Pi - \Pi S + B\Gamma = 0 \\
C\Pi + D_1 = 0
\end{cases}$$
(16)

where

$$C = \begin{bmatrix} 1 & 0 & 0 & 0 & 0 & 0 \\ 0 & 1 & 0 & 0 & 0 & 0 \\ 0 & 0 & 0 & 0 & 1 & 0 \end{bmatrix} D_1 = - \begin{bmatrix} 1 & 0 & 0 & 0 \\ 0 & 1 & 0 & 0 \\ 0 & 0 & 1 & 0 \end{bmatrix}$$

By solving Eq.(16) , the  ${\it II}$  and  ${\it \Gamma}$  can be sought as

$$\boldsymbol{\Pi} = \begin{bmatrix} 1 & 0 & 0 & 0 \\ 0 & 1 & 0 & 0 \\ 0 & s_1 & 0 & 0 \\ s_2 & 0 & 0 & 0 \\ 0 & 0 & 1 & 0 \\ 0 & 0 & 0 & 1 \end{bmatrix} \quad \boldsymbol{\Gamma} = \begin{bmatrix} s_1 s_2 - 2s_2 - 2\sigma_i - 1 & 0 & 0 \\ 0 & s_1 s_2 + 2s_1 - 1 + \sigma_i & 0 \\ 0 & 0 & -\omega_2^2 + \sigma_i \\ 0 & 0 & 0 \end{bmatrix}^{\mathrm{T}}$$

### 4 Simulation Results

In this section, the multi-layer triangular array formation is design based on the output regulation theory. The control laws described by Eqs. (14, 15) are applied to the motion equations for the Sun-Earth CRTBP. The Lagrange point is specified as  $L_1$ . The period and radius of the Sun-Earth system are  $T=365.26 \,\mathrm{d}$  and  $R_0=1.496\times 10^8 \,\mathrm{km} (=1 \,\mathrm{AU})$ , respectively. The remaining parameters are  $\rho =$  $3.0542 \times 10^{-6}$ ,  $\sigma_1 = 4.0611$ ,  $\sigma_2 = 3.9404$ ,  $\sigma_3 = 1$ , and  $a = 1 \times 10^{-5} \text{AU} \ (\approx 1.49 \times 10^{3} \text{ km})$ , and the phase angles of the equilateral triangular array formation are specified as  $[\tau_1, \tau_2, \tau_3] = [0^\circ, 120^\circ, 240^\circ]$ . To maintain the reference orbit, feedback control is essential. The feedback gain F for the feedback term in Eqs. (14, 15) can be chosen arbitrarily, provided that A - BF is asymptotically stable.

In this paper, the feedback gain is designed based on linear quadratic regulator theory, in which the gain is defined as  $F = R^{-1}\dot{B}X$ , with X being the solution of the Riccati equation (17), Q = I, and R = I. The fuel consumption  $\Delta V$  required to maintain this orbit in two periods is evaluated.

$$\dot{A}X + XA + Q - XBR^{-1}\dot{B}X = 0 \tag{17}$$

### 4. 1 Initialization of equilateral triangular array formation configuration

To ensure the initialization of the equilateral triangular array formation, the output regulation theory is used. The initial states of the spacecraft, denoted by  $\tilde{x}_i(0)$  ( $i = 1, 2, 3, \dots$ ), are given by

$$\tilde{x}_{i}(0) = [0,0,0,0,0,0]$$
 (18)

and the initial conditions  $\mathbf{w}_i(0)$  are given by

$$\begin{cases} \boldsymbol{w}_{i}(0) = [a\cos\tau_{i}, 2a\sin\tau_{i}, \sqrt{3} a\cos\tau_{i}, \\ -\sqrt{3} a\omega\sin\tau_{i}] \end{cases}$$

$$\tau_{i} = \left[0, \frac{2}{3}\pi, \frac{4}{3}\pi\right]$$

$$(19)$$

which is illustrated in Fig.3. Fig.3 illustrates the reference orbit generated by the exosystem, which provides the periodic signal required for the initialization of the triangular array formation.

To demonstrate that an equilateral triangular array formation is achieved, we define

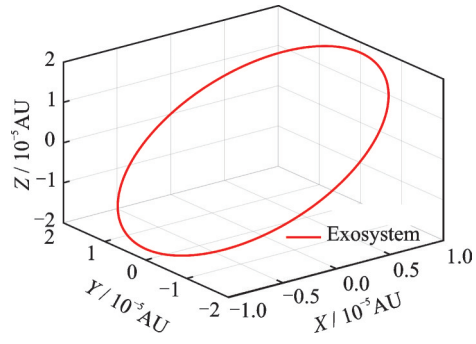


Fig.3 A circular orbit

$$d_{i}(t) = \sqrt{w_{ix}^{2}(t) + w_{iy}^{2}(t) + w_{iz}^{2}(t)}$$

$$i = 1, 2, 3$$
(20)

An equilateral triangular array formation is shown in Fig.4 and Fig.5, which show the two-layer and three-layer equilateral triangular array formations, respectively. These results demonstrate that equilateral triangular array formation is formed in two periods owing to the output regulation.

The error histories are shown in Figs. 6,7 (only illustrated the two-layer equilateral triangular array formation). The errors converge to zero, indicating that the spacecraft finish the initialization process and maintain it according to the control law.

As time progresses,  $d_i$  converges to constant values (Figs. 8, 9), thereby demonstrating the estab-

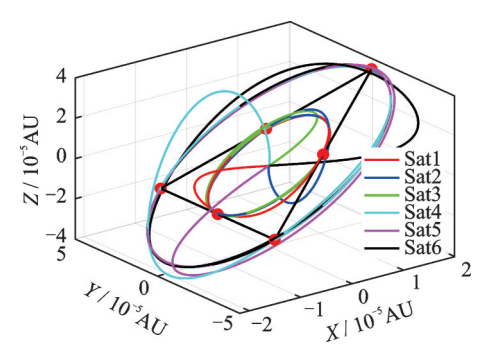


Fig.4 Two-layer equilateral triangular array formation for nonlinear system

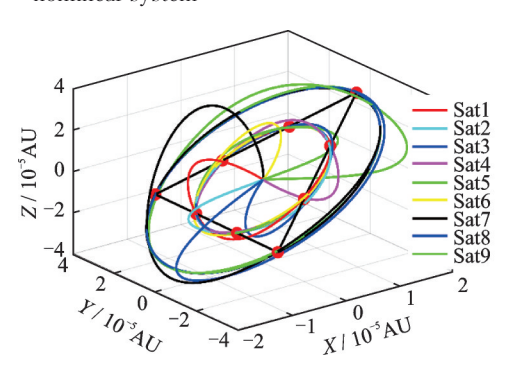


Fig.5 Three-layer equilateral triangular array formation for nonlinear system

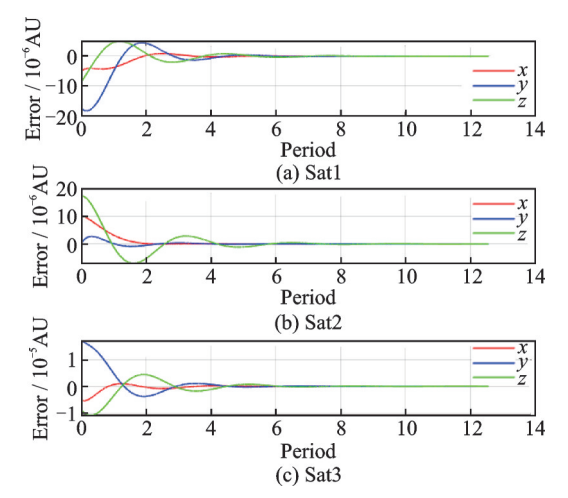


Fig.6 Errors for two-layer equilateral triangular array formation for nonlinear system (in-circle)

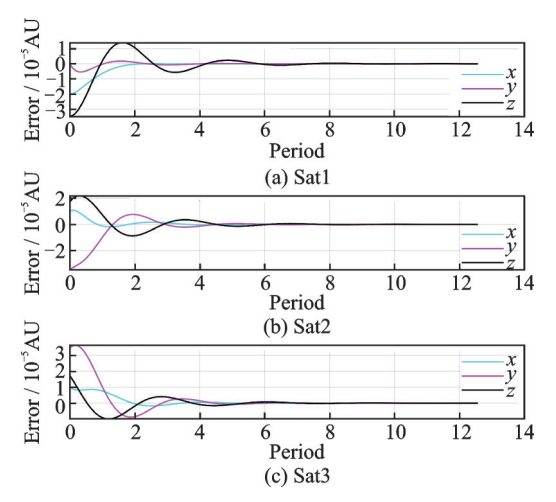
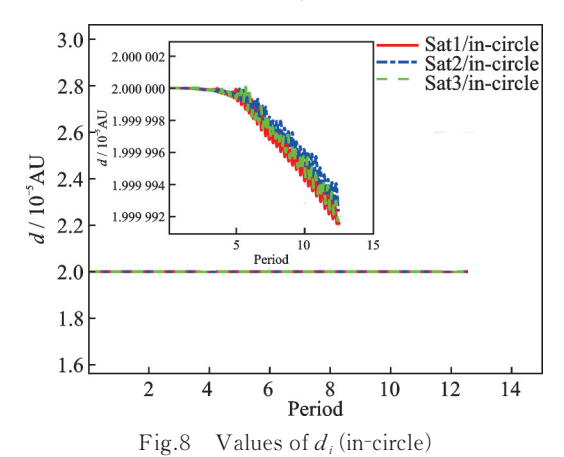


Fig.7 Errors for two-layer equilateral triangular array formation for nonlinear system (out-circle)



lishment of an equilateral triangular array formation.

Next, using the coordinate system centered at Lagrange points  $L_1, L_2, L_3$  calculate the  $\Delta V$  ( $L_1$ -norm of control input), as is shown in Fig.10 (only calculate one-layer equilateral triangular formation).

In Fig.10, the  $\Delta V$  values of three spacecraft

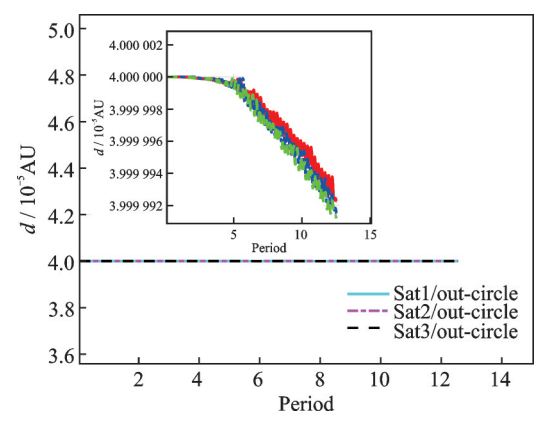


Fig.9 Values of  $d_i$  (out-circle)

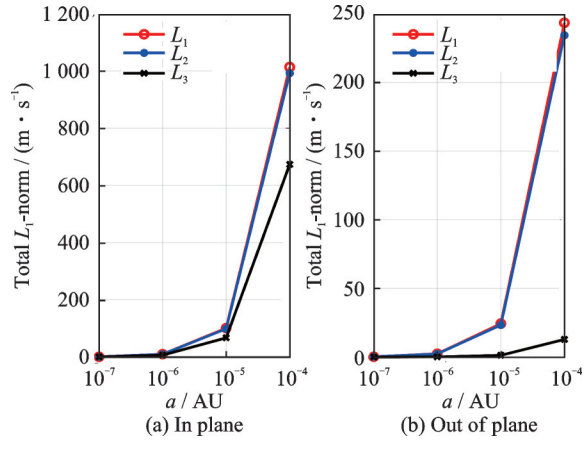


Fig. 10 Total values of  $L_1$ -norm for nonlinear system

centered at Lagrange points  $L_1$  and  $L_2$  are shown to be larger than those at Lagrange point  $L_3$ . When  $a=10^{-4}{\rm AU}~(\approx 1.49\times 10^4~{\rm km})$ , the maximum values are 1 013 m/s (for Lagrange point  $L_1$ ), 991.9 m/s (for Lagrange point  $L_2$ ), 673.3 m/s (for Lagrange point  $L_3$ ) for in plane, respectively. As for out of plane, the maximum values are 243.4 m/s (for Lagrange point  $L_1$ ), 234.3 m/s (for Lagrange point  $L_2$ ), 12.87 m/s (for Lagrange point  $L_3$ ), respectively.

Lagrange points  $L_1$  and  $L_2$  are located on the side of the Earth, where both the points balance the gravitational force of the Sun and the Earth. Although they are equilibrium points, spacecraft at these locations require more fuel to maintain stability because the difference in gravitational forces from the Sun and Earth is significant. In contrast, Lagrange point  $L_3$  is located on the opposite side of Earth's orbit, farther from the influence of both the Sun and Earth. Although this point also balances the gravitational forces of the Sun-Earth system, the

spacecraft at Lagrange point  $L_3$  experience less gravitational perturbation from external sources, thereby requiring less fuel to maintain formation stability. Positioned on the far side of the Sun-Earth system, this point is more stable and subject to fewer external disturbances. According to the CRTBP, Lagrange points  $L_1$  and  $L_2$  are unstable equilibrium points and Lagrange point  $L_3$  is also unstable. However, its degree of instability is slightly lower compared with Lagrange points  $L_1$  and  $L_2$ . Although Lagrange point  $L_3$  is not a fully stable point, the reduced external disturbances make it easier to maintain stability, thus requiring less control input.

### 4. 2 Natural stability analysis of uncontrolled equilateral triangular array formation

In Section 4.1, the configuration design and initialization control of the equilateral triangular array formation were accomplished, ensuring that the three spacecraft establish a strict equilateral triangular array formation under the output regulation theory. Nevertheless, in GWO missions, the propulsion system must be deactivated during the scientific phase in order to avoid non-inertial disturbances induced by continuous thrust, such that the spacecraft remain in a pure state for accurate interferometric measurements of GW signals. Consequently, to guarantee the feasibility and continuity of the observation mission, it is essential to systematically evaluate the geometric and dynamical stability of the formation without control input, thereby identifying the intrinsic timescale of natural configuration maintenance as well as the appropriate timing for control intervention.

In actual mission operations, continuous control not only introduces non-inertial disturbances but also increases fuel consumption. Therefore, once initialization is completed, the spacecraft typically enter a "natural drift" phase, during which short-term observational capability relies on the intrinsic dynamical stability of the triangular configuration. Accordingly, this section investigates the evolution of the equilateral triangular array formation after initialization under the Sun-Earth CRTBP dynamical model, without using any control input. By

comparing with the performance requirements of the LISA mission, it is noted that, during the scientific phase, the variation in arm length is typically maintained within 1.5%-2% of its nominal value<sup>[11]</sup>, in order to ensure interferometric measurement accuracy.

Therefore, this section systematically analyzes the natural stability of the equilateral triangular formation from two perspectives.

# 4. 2. 1 Analysis of arm-length evolution of the equilateral triangular array formation without control input

This section investigates the temporal evolution of the three arm lengths of the formation, aiming to evaluate the capability of the equilateral triangular array formation configuration and preserve its geometric structure without control input. To ensure the ranging accuracy of the observation, the stability of the formation must be constrained within 2\% according to the requirements of GWO. Among these parameters, the arm length serves as the fundamental baseline of the interferometer, and its relative variation directly reflects the integrity and stability of the formation. In GWO missions, if the variation in the inter-spacecraft arm length exceeds 2% of the nominal value, the interferometric measurement accuracy is severely degraded, and the formation is generally regarded as having failed. Therefore, by tracking the time history of the arm length variations and identifying the first instance when the threshold is exceeded, the natural maintenance duration of the formation can be quantified, thereby providing a theoretical basis for the scheduling of control interventions.

In the natural stability analysis conducted in this section, the formation radius is set to  $a=10^{-5}\,\mathrm{AU}$ , which corresponds to approximately 1 490 km. The resulting arm length of the equilateral triangular array formation is about 2 581.99 km. Considering the stability requirements of GWO missions, this study adopts the same as the LISA mission, namely that the arm length variation must not exceed 2%. Accordingly, the maximum allowable arm length deviation is determined as follows

$$\Delta L_{\text{max}} = 2\% \times L \tag{21}$$

where  $\Delta L_{\rm max}$  denotes the maximum arm length variation and L the nominal arm length of the equilateral triangular array formation. The calculated maximum variation is 51.64 km, which is adopted as the critical threshold for determining formation failure. Once the actual distance variation between any two spacecraft exceeds it, the formation is regarded as invalid, as it can no longer meet the baseline stability required for interferometric measurements.

Fig.11 illustrates the arm length variation between the three spacecraft (only show one-layer). At the initial state, all arm lengths are approximately 2581.99 km. According to the stability criterion, the maximum allowable arm-length variation is within  $\pm 2\%$ , that is,  $L_{\rm min} \approx 2530.35$  km and  $L_{\rm max} \approx 2633.63$  km. Once the distance between any two spacecraft without control input exceeds  $L_{\rm min}$  or  $L_{\rm max}$ , the formation is considered to have lost the geometric stability required for interferometric measurements.

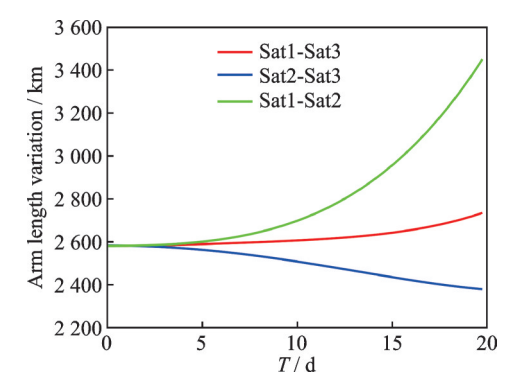


Fig.11 Arm length variation (only show one-layer)

As shown in Fig.11, the distance between Sat1 and Sat2 increases most rapidly and first exceeds the upper bound of 2 633.63 km at  $T\!=\!7.552$  d. In contrast, the arm length between Sat2 and Sat3 gradually decreases and reaches the lower bound of 2 530.35 km at  $T\!=\!8.132$  d. Since the criterion for formation failure is defined as the first crossing of the tolerance threshold by any arm, the effective stability duration of the formation under uncontrolled conditions is determined to be  $T_{\rm stable}\!=\!7.552$  d.

This result indicates that, during the natural drift of the three spacecraft without control input, the stability of the equilateral triangular array forma-

tion is limited. Therefore, control correction is required approximately every 7.552 d to ensure the continuity of the GWO mission.

## 4. 2. 2 Evolution of equilateral triangular array formation deviation under uncontrolled conditions

As indicated in Section 4.2.1 on arm length variations, under uncontrolled conditions the formation arm lengths rapidly deviate from their initial values, exceeding the tolerance threshold in approximately 7.552 d and leading to formation failure. Although arm length variation effectively characterizes the overall stability boundary of the formation and serves as the primary criterion for mission tolerance, this metric mainly reflects the relative geometric relationships among the spacecraft. It does not, however, reveal the absolute deviations of each spacecraft from their nominal trajectories under uncontrolled conditions. Therefore, to more comprehensively evaluate formation stability, it is necessary to further analyze the position errors of each spacecraft relative to the initialized reference orbit.

As shown in Fig.12, under uncontrolled conditions the three spacecraft exhibit significant orbital deviations after approximately 7.552 d (i.e., when the formation fails), with the deviations occurring primarily along the X-axis (the Sun-Earth direction). Specifically, at 7.552 d of natural drift, the maximum deviation of Sat1 along the X-axis reaches 180.7 km, while those of Sat2 and Sat3 are -89.92 and -90.82 km, respectively. The deviations of the three spacecraft are opposite in direction but comparable in magnitude, indicating a strongly divergent trend along the X-axis. This result demonstrates that, near the Sun-Earth Lagrange point  $L_1$ , the instability in the X-axis dominates the evolution of the formation.

In the Sun-Earth system, the Lagrange point  $L_1$  is a typical saddle equilibrium position, whose stability characteristics can be analyzed by linearization under the CRTBP. After linearizing the system near Lagrange point  $L_1$ , the corresponding Jacobian matrix consists of one pair of real eigenvalues  $\pm \lambda$  and two pairs of purely imaginary conjugate eigen-

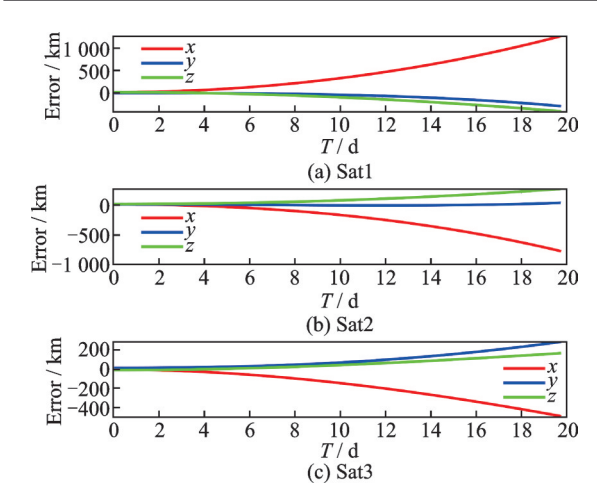


Fig.12 Evolution of formation deviation under uncontrolled conditions (only show one-layer)

values  $\pm i\omega_1$  and  $\pm i\omega_2$ . The real eigenvalues correspond to directions aligned with the Sun-Earth direction (i.e., the X-axis direction), implying that any small perturbation along this direction will enlarge exponentially within the unstable subspace without control input. This dynamical mechanism fundamentally explains why the deviations of the spacecraft are most divergent along the X-axis and why the formation configuration fails first in this direction.

Above all, the results show that, without optimization, the equilateral triangular array formation maintains its stability for about 7.5 d under uncontrolled conditions. This interval is noticeably shorter than the correction cycles reported in established missions such as LISA, suggesting a higher frequency of intervention. However, it should be emphasized that the present result is obtained without any optimization of orbital parameters, initial conditions, or control strategies, indicating substantial potential for further improvement. More importantly, this study represents the first extension of formation stability and maintenance analysis to arbitrary orbital environments, rather than being confined to traditional heliocentric or specific mission orbits. This not only demonstrates the universality and feasibility of the proposed approach but also provides new theoretical insights and technical references for future GWO missions in diverse orbital scenarios, thereby carrying significant importance.

### 4. 3 Reconfiguration control of equilateral triangular array formation

To ensure the long-term stability of GWO, formation reconfiguration control is an inevitable requirement. The dynamic nature of GWO mission demands imposes more flexible and adaptive requirements on the configuration. These requirements are reflected in two main aspects. On one hand, as the frequency band of GWs in a fixed direction changes, the inter-spacecraft distance must be dynamically adjusted to optimize the interferometric sensitivity for different frequency bands and this type is referred to as scale reconfiguration. On the other hand, when the position or direction of the GW source changes, the orbital plane of the formation must be adjusted accordingly to achieve optimal pointing for observation. This type of reconfiguration is referred to as pointing reconfiguration. This study primarily focuses on scale reconfiguration.

When observing GWs of different frequencies from the same direction, configuration reconfiguration control is required.

During the implementation of scale reconfiguration, a scaling factor  $\lambda$  is introduced, and the configuration position vectors are expanded or contracted as

 $\mathbf{w}_{\text{scale}}(t) = \lambda \cdot [\mathbf{w}_1(t) \ \mathbf{w}_2(t) \ \mathbf{w}_3(t)] \ \lambda > 0 \ (22)$  where  $\lambda$  determines the scale reconfiguration. When  $\lambda > 1$ , the formation enlarges and the inter-spacecraft distances increase, leading to an extended arm length that is favorable for observing low-frequency GWs. Conversely, when  $\lambda < 1$ , the formation contracts, which is suitable for high-frequency GWs.

During the formation scaling adjustment, the inter-spacecraft relative distance varies with  $\lambda$ , and can be expressed as

$$d_{ij}^{\text{scale}}(t) = |w_i^{\text{scale}}(t) - w_j^{\text{scale}}(t)| = \lambda |w_i(t) - w_j(t)|$$
  

$$i = 1, 2, 3; \quad j = 1, 2, 3; \quad i \neq j$$
 (23)

As shown in Eq.(23), the scale reconfiguration process is directly reflected as a proportional change in the inter-spacecraft distances, while the geometric similarity of the formation remains unchanged.

In Fig.13, when GWs from the same direction

are relatively weak, it becomes necessary to perform scale reconfiguration. This process involves adjusting the triangular formation by expanding its configuration under the application of control forces. In Fig.14, when GWs from the same direction are relatively strong, it also becomes necessary to perform scale reconfiguration by contracting its configuration under the application of control forces. It allows the triangular formation to maintain optimal sensitivity and detection capability, ensuring that the triangular formation is appropriately aligned to observe the weaker GWs.

While scale expansion in GWO missions is primarily intended to enhance sensitivity to low-frequency and weak signals, scale contraction is not "unnecessary". The key lies in the distinct response of interferometric measurements across different frequency bands. When the arm length becomes too long, high-frequency signals may experience excessive phase differences between spacecraft, leading to phase decorrelation and reduced measurement effectiveness. Thus, the purpose of scale contraction is not to address "strong" GWs, but rather to adapt the formation to high-frequency

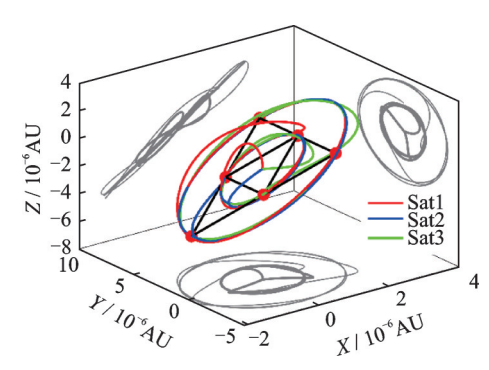


Fig.13 One-layer equilateral triangular formation configuration reconfiguration ( $a = 10^{-6} \text{AU}, \lambda = 3$ )

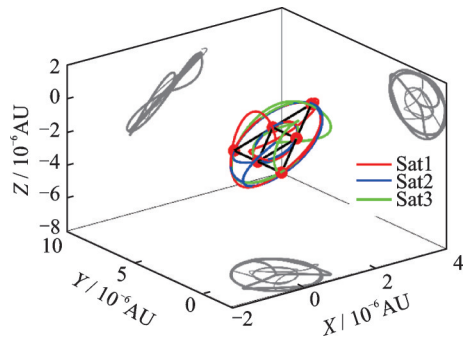


Fig.14 One-layer equilateral triangular formation configuration reconfiguration ( $a = 10^{-6} \text{AU}, \lambda = 0.5$ )

signals, ensuring optimal signal-to-noise ratio and measurement precision in that regime. From a mission design perspective, scale reconfiguration is not envisioned as a frequent operation but as a limited, stage-specific adjustment. By predefining a small number of scaling maneuvers within the mission plan, it is possible to balance scientific return with propellant consumption, thereby preserving mission feasibility while significantly extending the accessible frequency range.

### 5 Conclusions

An equilateral triangular array formation initialization near Lagrange point  $L_1$  is examined. To establish the equilateral triangular array formation and maintain it in two periods, the tracking aspect of output regulation theory is employed. For the equilateral triangular array formation, the reference trajectory is generated by an exosystem. Then, the equilateral triangular array formations are established and maintained. The errors are calculated, demonstrating that the equilateral triangular array formation is well-maintained. In addition, to evaluate the formation configuration after initialization under uncontrolled conditions, a natural stability analysis is conducted. The results show that, with an orbital radius of a = 1490 km, the arm length of the formation exceeds the tolerance of 2\% within approximately 7.552 d, indicating the onset of configuration failure. The deviations of the three spacecraft are most pronounced along the X-axis (the Sun-Earth direction), reflecting the inherent dynamical instability of the Lagrange point  $L_1$  in this direction. Subsequently, the fuel consumption for the formation initialization at the Lagrange points  $L_1, L_2$ , and  $L_3$  are calculated, respectively. It is found that the fuel consumption required at the Lagrange point  $L_3$  is significantly lower than that at other points. Finally, when observing GWs from the same direction with different frequency bands, configuration scale reconfiguration control is performed.

### References

[1] NI W T. Gravitational wave detection in space[J]. International Journal of Modern Physics D, 2016, 25 (14): 1630001.

- [2] QIAO D, JIA F D, LI X Y, et al. A review of orbital mechanics for space-based gravitational wave observatories[J]. Space: Science & Technology, 2023, 3: 15.
- [3] ABRAMOVICI A, ALTHOUSE W E, DREVER R W P, et al. LIGO: The laser interferometer gravitational-wave observatory[J]. Science, 1992, 256(5055): 325-333.
- [4] ANDO M, COLLABORATION T T. Current status of the TAMA300 gravitational-wave detector[J]. Classical and Quantum Gravity, 2005, 22(18): S881-S889.
- [5] WILLKE B, AUFMUTH P, AULBERT C, et al. The GEO 600 gravitational wave detector[J]. Classical and Quantum Gravity, 2002, 19(7): 1377.
- [6] DANZMANN K. LISA mission overview[J]. Advances in Space Research, 2000, 25(6): 1129-1136.
- [7] KAWAMURA S, ANDO M, SETO N, et al. The Japanese space gravitational wave antenna: DECIGO[J]. Classical and Quantum Gravity, 2011, 28(9): 094011.
- [8] CORBIN V, CORNISH N J. Detecting the cosmic gravitational wave background with the Big Bang Observer[J]. Classical and Quantum Gravity, 2006, 23 (7): 2435-2446.
- [9] CHENG J, LI E K, HU Y M, et al. Detecting the stochastic gravitational wave background with the TianQin detector[J]. Physical Review D, 2022, 106 (12): 124027.
- [10] LUO Z R, GUO Z K, JIN G, et al. A brief analysis to Taiji: Science and technology[J]. Results in Physics, 2020, 16: 102918.
- [11] FOLKNER W M, HECHLER F, SWEETSER T H, et al. LISA orbit selection and stability[J]. Classical and Quantum Gravity, 1997, 14(6): 1405-1410.
- [12] NAYAK K R, KOSHTI S, DHURANDHAR S V, et al. On the minimum flexing of LISA's arms[J]. Classical and Quantum Gravity, 2006, 23(5): 1763-1778.
- [13] DE MARCHIF, PUCACCOG, BASSAN M. Optimizing the earth-LISA "rendezvous" [J]. Classical and Quantum Gravity, 2012, 29(3): 035009.
- [14] JIAO B H, DANG Z H. Formation design of for space gravitational wave detection based on second order cw equation[J]. Journal of Deep Space Exploration, 2023, 10(3): 257-267.
- [15] LIU P D, JIAO B H, DANG Z H. Design method of polygon formation for space-based gravitational-wave detection[J]. Acta Aeronautica et Astronautica Sinica, 2022, 43(S1): 526907.
- [16] XIA Y, LIGY, HEINZELG, et al. Orbit design for the laser interferometer space antenna (LISA)[J]. Science China Physics, Mechanics and Astronomy, 2010, 53(1): 179-186.

- [17] XIE X, JIANG F H, LI J F. Design and optimization of stable initial heliocentric formation on the example of LISA[J]. Advances in Space Research, 2023, 71 (1): 420-438.
- [18] WU A M, NI W T. Deployment and simulation of the astrod-gw formation[J]. International Journal of Modern Physics D, 2013, 22(1): 1341005.
- [19] SABERI A, STOORVOGEL A, SANNUTI P. Control of Linear Systems with Regulation and Input Constraints[M]. London: Springer London, 2000.
- [20] BANDO M, ICHIKAWA A. Formation flying along halo orbit of circular-restricted three-body problem[J]. Journal of Guidance, Control, and Dynamics, 2015, 38(1): 123-129.
- [21] AKIYAMA Y, BANDO M, HOKAMOTO S. Station-keeping and formation flying based on nonlinear output regulation theory[J]. Acta Astronautica, 2018, 153: 289-296.
- [22] SHOUMAN M, BANDO M, HOKAMOTO S. Performance analysis of low-gain feedback for saturated differential drag in a high-precision orbit propagator[J]. Transactions of the Japan Society for Aeronautical and Space Sciences, 2020, 63(5): 243-247.

**Acknowledgement** This work was supported by the China Scholarship Council (CSC)(No.202206290131).

#### Authors

The first author Dr. PAN Zhengxu received his Ph.D. degree in flight vehicle design from Northwestern Polytechnical University, Xi'an, China, in 2025. His research interests are spacecraft formation flying, orbital dynamics and control methods.

The corresponding author Prof. ZHU Zhanxia received the B.S., M.S., and Ph.D. degrees from Northwestern Polytechnical University, Xi' an, China, in 1995, 1998, and 2002, respectively. Her research interests include spacecraft orbital dynamics, space operations and control.

Author contributions Dr. PAN Zhengxu developed the methodology and prepared the original manuscript draft. Prof. BANDO Mai conceptualized the study and contributed to the review and editing of the manuscript. Prof. ZHU Zhanxia conceptualized the study and contributed to the review and editing of the manuscript. Prof. HOKAMOTO Shinji developed the methodlogy and contributed to the review and editing of the manuscript. All authors commented on the manuscript draft and approved the submission.

**Competing interests** The authors declare no competing interests.

### 天基引力波探测等边三角形阵列编队构形初始化控制

潘政旭<sup>1</sup>, BANDO Mai<sup>2</sup>, 朱战霞<sup>1</sup>, HOKAMOTO Shinji<sup>2</sup>

(1.西北工业大学航天学院,西安710072,中国; 2.九州大学航空航天系,福冈819-0395,日本)

摘要:分析了圆形限制性三体问题中拉格朗日点附近的天基引力波探测(Gravitational wave observatory, GWO)等边三角形阵列编队初始化问题。稳定的编队构型对于引力波(Gravitational waves, GWs)的连续探测至关重要,然而共线平动点附近的运动极不稳定。鉴于此,本文利用输出调节理论对该问题进行了研究。利用输出调节理论中的轨迹跟踪方法,在两个周期内建立等边三角形阵列编队并进行了构型保持,同时计算了燃料消耗。此外,分析了无控状态下等边三角形阵列编队的自然演化过程,量化了有效探测的持续时间,以确定控制干预的时机。最后,为了探测同一方向不同频段的引力波,进行了编队尺度重构控制。

关键词:天基引力波探测;等边三角形阵列编队初始化;拉格朗日点;输出调节理论